Fully Conformal Square-Patch Frequency-Selective Surface Toward Wearable Electromagnetic Shielding

Praveen Gurrala, Seval Oren, Peng Liu, Jiming Song, and Liang Dong

***Abstract*—This letter reports on a fully conformal square-patch frequency-selective surface (FSS) consisting of liquid metal alloy embedded within a flexible silicone elastomer. The flexible and elastic nature of the FSS provides high conformity to doubly curved surfaces. The transmission properties of the FSS on both singly and doubly curved surfaces are studied. This FSS can facilitate electromagnetic interference reduction in the X-band frequency range when wrapped on cylindrical or spherical radomes over dipole-like antennas, thus surpassing many existing flexible FSS technologies that usually allow conformable contact only with singly curved surfaces.**

***Index Terms*—Electromagnetic (EM) interference, frequency-selective surfaces (FSSs), spatial filters.**

I. Introduction

A TYPICAL frequency-selective surface (FSS) has a planar structure with periodically arranged cells made of metallic elements to reflect or transmit electromagnetic (EM) waves at certain frequencies. The frequency-filtering properties of the FSS have inspired their use in many applications such as multiband satellite communication, EM interference shielding, hybrid radomes [1, Ch. 1], radar-absorbent materials, and artificial magnetic conducting surfaces. Frequency-tunable FSSs with dynamic capacitive loads have also been developed [2] using microelectromechanical systems (MEMS) and sophisticated microfabrication techniques [3]. The shape and size of the metallic elements of the FSS determine its reflection and transmission characteristics. Recently, conformal FSSs have attracted considerable attention for wearable frequency-selective EM shielding and communication applications that often desire low-profile and high-flexibility features of such FSSs. Although FSSs formed on conventional flexible substrates have allowed conformity to singly curved surfaces, they do not easily conform to doubly curved surfaces because the substrate and conducting elements of the FSS are not both stretchable. When such FSSs are used on any doubly curved surfaces, unfavorable cut-and-paste discontinuities will be introduced. This emphasizes the need for conformable FSSs made with all flexible and stretchable materials.

Flexible FSSs have been developed using inkjet printing [4], screen printing [5], and the MEMS method [6]. Progress has also been made in fabrication of textile FSSs by either knitting, weaving, or printing [7]. A flexible FSS with miniaturized elements has also been reported [8]. It should be noted that most of the existing curved FSSs were formed on flexible yet inelastic substrates such as rigid-flex Kapton or cotton textile. Although FSSs and other flexible EM devices based on elastic substrates have recently been reported in [9]–[12], conformable wrapping of flexible FSSs onto doubly curved surfaces without introducing discontinuities is still challenging.

In this letter, we report on a fully conformal FSS consisting of square liquid metal patches embedded inside a stretchable elastomer. This FSS acts as a conformal low-pass filter when wrapped on cylindrical or spherical radomes over dipole antennas. The fluid nature of liquid metal and the stretchability of the elastomer allow the FSS to be conformably wrapped on doubly curved surfaces without introducing any discontinuities. We demonstrate that the conformal FSS has an ability to reduce EM interference in the X-band frequency range.

II. Design and Fabrication

Our interest is to develop a conformal FSS that acts as a low-pass filter to shield sensitive equipment operating in the ISM band (below 2.4 GHz) from radiating higher frequency power. The goal is to obtain at least 10 dB attenuation in the X-band. Designing such a conformal FSS is challenging because, unlike planar doubly periodic FSSs, curved FSSs are not easily amenable to efficient analysis. Analytical methods for full-wave analysis of curved FSSs of simple shapes [13] can be used as a design basis. Alternatively, an easier approach to the design of curved FSSs is to use approximation techniques, such as ray tracing, to analyze the effect of curvature. We adopted this approach in this work. The electric field transmitted into a curved FSS is approximately proportional to the transmission coefficient of the corresponding infinite planar FSS, as will be shown later using ray theory approximations. Therefore, we designed our FSS based on the transmission properties of an infinite planar FSS.

To achieve a low-pass transmission response, we chose nonresonant elements in our design because of the following disadvantages with low-frequency resonant elements [1, Ch. 1]. First, for the elements to exhibit resonance at the desired frequency, their size must be comparable to half a wavelength, which is considerably large for low frequencies. Second, the elements of the FSS may exhibit higher order resonances in the X-band, causing undesirable transmission/reflection responses at those frequencies. Most importantly, multiple grating lobes may also exist at some angles of incidence because of the large periodicity. Therefore, for a low-pass transmission response, we chose a periodic square-patch FSS with element dimensions much smaller than the wavelength of operation (frequency < 3 GHz). Such periodic surfaces are known to have a capacitive surface impedance [14] and, therefore, act as low-pass filters. The square metallic patches are made of eutectic gallium–indium (EGaIn: 75.5% gallium and 24.5% indium), a liquid metal at room temperature [10]. Dimensions of the

Manuscript received March 2, 2017; revised June 30, 2017; accepted July 23, 2017. Date of publication August 2, 2017; date of current version September 18, 2017. This work was supported in part by the U.S. National Science Foundation under Grant ECCS-0954765. The work of S. Oren was supported by the Turkish Council of High Education and Anadolu University, Turkey. *(Corresponding authors: Jiming Song; Liang Dong.)*

The authors are with the Department of Electrical and Computer Engineering, Iowa State University, Ames, IA 50011 USA (e-mail: praveeng@iastate.edu; soren@iastate.edu; pengliu@iastate.edu; jisong@iastate.edu; ldong@iastate.edu).

Color versions of one or more of the figures in this letter are available online at http://ieeexplore.ieee.org.

Digital Object Identifier 10.1109/LAWP.2017.2735196

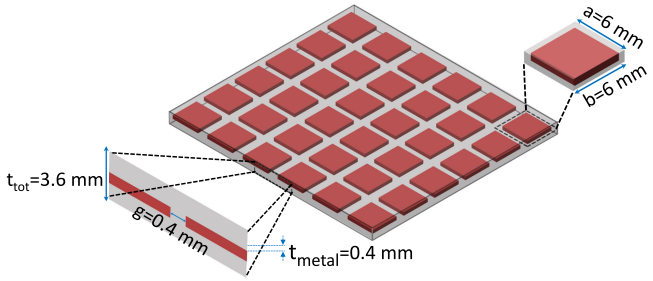

Fig. 1. Schematic of the FSS with dimensions shown in the inset.

TABLE I
DIMENSIONS OF THE FSS AT DIFFERENT LEVELS OF STRAIN

Strain	G_x	G_y	H	L_x	L_y	T
8%	0.42	0.4	0.37	5.6	6.48	3.58
14.8%	0.4	0.42	0.35	5.46	6.89	3.45
21.5%	0.38	0.43	0.34	5.33	7.29	3.33
28.1%	0.35	0.44	0.33	5.21	7.69	3.23
34.8%	0.33	0.45	0.32	5.09	8.09	3.07

All values are in millimeters. The direction of stretching is the y-axis with the FSS lying in the xy plane. The gap between the metal patches and the length of each patch along the x- and y-directions are represented by G_x, G_y, L_x, and L_y, respectively. Thickness of the metal patch and the substrate are H and T, respectively.

patches are shown in Fig. 1 and were chosen using simulations performed in HFSS to achieve at least 15 dB attenuation from 8 to 12 GHz. We will show that stretching the FSS leads to changes smaller than 5 dB in the transmission coefficient so that the design goal of 10 dB attenuation is satisfied. The liquid metal EGaIn is embedded inside a 3.6 mm thick stretchable silicone elastomer Ecoflex 00-30. The metal patches are located nearly at the center of the elastomer. The fabrication process flow for the FSS follows [10]. The dielectric constant and loss tangent of the elastomer are 2.5 and 0.1, respectively [11]. Mechanical properties of the elastomer can be obtained from [15].

The transmission characteristics of the infinite doubly periodic planar FSS were studied first using unit cell simulations in HFSS. Master–slave boundary conditions were used on the four sides of the unit cell to simulate the periodic structure. An incident plane wave was set normal to the plane of the FSS because the measured transmission response can be approximately related to the transmission coefficient of the planar FSS at normal incidence, as will be shown in Section III. In order to examine the effect of stretching the FSS along a single direction on the transmission coefficient, the simulation was carried out with the measured key dimensions of the device (see Table I) at different stretch levels, and the magnitude of transmission coefficient at each stretch level is plotted in Fig. 2. It is shown that at frequencies below 2 GHz, the maximum change in the transmission coefficient caused by stretching is less than 2.5 dB. However, asymmetric stretching of the FSS introduces differences in the transmission coefficients of different polarizations. For comparison, the difference in the magnitude of the transmission coefficient for two different polarizations (electric field along x- or y-axis) at normal incidence is plotted in Fig. 3. At low frequencies and for small strains, the difference in the transmission coefficients is insignificant. However, as the strain increases, a difference of as much as 2 dB can be seen even at 2 GHz. These differences may lead to deviations from the desired transmission response in some applications where significant asymmetric stretching of the FSS

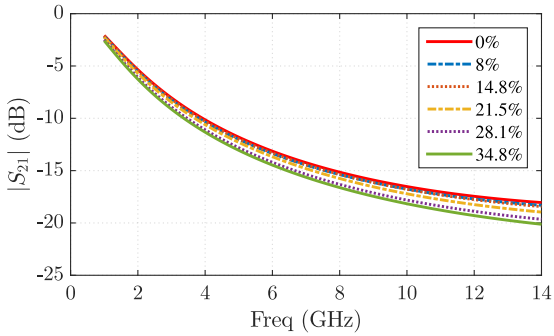

Fig. 2. Transmission coefficient of the planar FSS at normal incidence for different stretch levels, with 0% standing for the unstretched state.

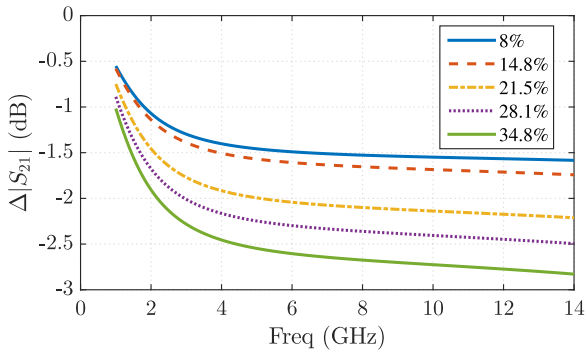

Fig. 3. Difference in the transmission coefficient of the planar FSS for two different polarizations at normal incidence for different stretch levels.

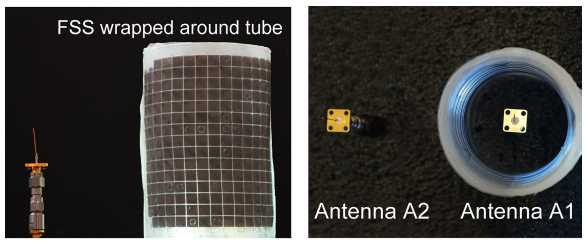

Fig. 4. Experimental setup for measuring the transmission coefficient of the FSS when it is wrapped on a cylindrical paper tube. (a) FSS wrapped around a tube. (b) Position of the antennas relative to the FSS.

is involved. From the simulation results, it is expected that the planar FSS acts as a low-pass filter with at least 10 dB attenuation from 8 to 12 GHz.

III. EXPERIMENTAL RESULTS AND DISCUSSION

Fig. 4 shows the setup for testing the transmission response of the FSS wrapped on a cylindrical surface. Two identical monopole antennas (each 21 mm long) were placed at a separation of 94 mm. The S-parameters of this pair of antennas were measured under the following conditions.

1) The antennas radiate in free space.
2) A bare cylindrical paper tube covers antenna A1 lining up with the central axis of the cylinder.
3) The FSS covers the cylindrical paper tube over the antenna.

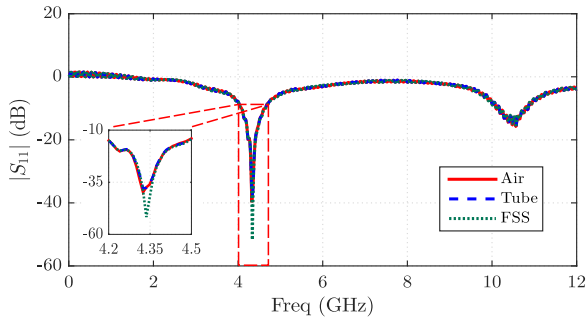

Fig. 5. $|S_{11}|$ under different conditions. Solid line: Antenna radiating in free space. Long dashed line: Antenna covered by a bare paper tube. Short dashed line: Antenna covered by a bare paper tube that is covered with the FSS.

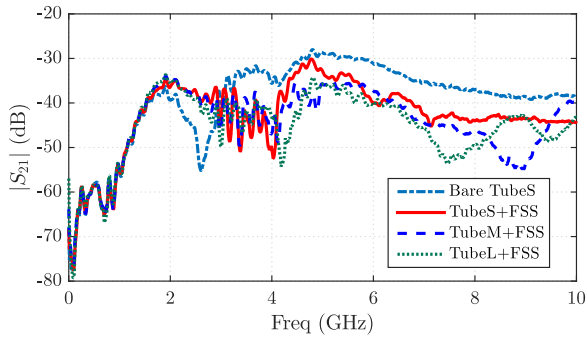

Fig. 6. Measured $|S_{21}|$ when tubes of different radii are covered by the FSS.

In the experiment, three tubes of different radii (19.7, 25.7, and 36.5 mm) were used, and for each of these tubes, the S-parameters were obtained under the above three conditions. The three tubes are called TubeS, TubeM, and TubeL in the increasing order of radius. Fig. 5 shows $|S_{11}|$ of the pair of antennas under the three conditions for TubeS. Since the antennas are identical, the values of $|S_{22}|$ under all the three conditions are equal to the values of $|S_{11}|$ obtained when antenna A1 is radiating in free space. Fig. 5 shows that the antennas radiate at two frequencies: 4.4 and 10.6 GHz. Also, placing the tube (bare or with FSS) around antenna A1 has no effect on $|S_{11}|$, indicating that no coupling exists between the antenna and the tube.

Fig. 6 shows the frequency variation of $|S_{21}|$ with the FSS wrapped on the surfaces of different tubes. When antenna A1 was covered by TubeS but without the FSS, the obtained value of $|S_{21}|$ serves as a reference. Only the measurements below 10 GHz are shown because the observed value of $|S_{21}|$ beyond 10 GHz was less than 40 dB even when the antennas were radiating in free space. Fig. 6 indicates that the FSS attenuates high-frequency signals starting around 3 GHz. To quantitatively evaluate the effect of the FSS, the change in $|S_{21}|$ introduced by the FSS ($|S_{21}|$ with FSS $-$ $|S_{21}|$ without FSS) wrapped on the tube is plotted in Fig. 7. Let S be the value of $|S_{21}|$ without the FSS and S_F be the value of $|S_{21}|$ with the FSS. Then, Fig. 7 is meaningful only for the frequencies where either S_F or S is significantly above the background noise level. For example, both S_F and S are close to the background noise level at very low frequencies, and their difference at these frequencies carries no information of the transmission response of the FSS. From Fig. 6, the frequencies where either S_F or S is significant can be identified. Looking at the difference in $|S_{21}|$ at these frequencies in Fig. 7, the FSS can be seen to exhibit a low-pass

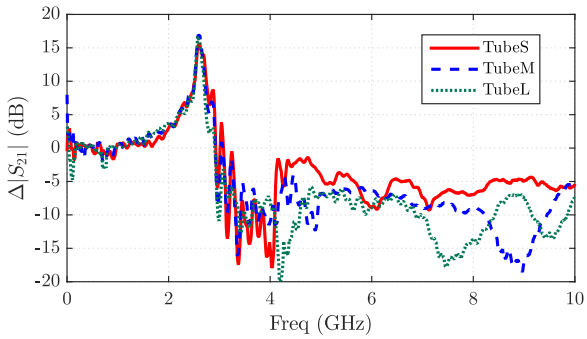

Fig. 7. Difference in $|S_{21}|$ introduced by the FSS for each of the letter tubes.

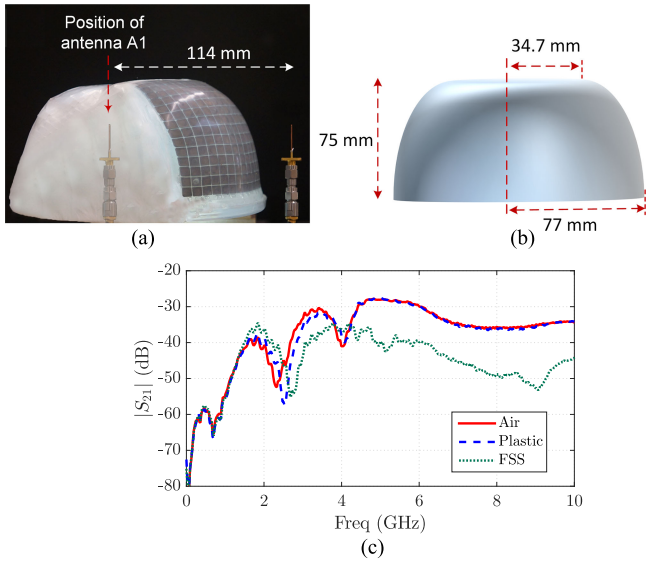

Fig. 8. (a) Optical image of FSS wrapped plastic bowl with two antennas A1 (overlaid image) and A2, inside and outside of plastic bowl, respectively. (b) Schematic showing the dimensions of the plastic bowl. (c) Measured value of $|S_{21}|$ under different conditions. Solid line: Antenna radiating in free space. Dashed line: Antenna A1 is covered with a plastic bowl. Dotted line: Antenna A1 is covered with a plastic bowl wrapped with FSS.

transmission response, with at least 5 dB of attenuation from 6 to 10 GHz, irrespective of the radius of the tube.

To characterize the performance of the FSS on a doubly curved surface, we performed a measurement using an approximately spherically curved polyethylene plastic surface [see Fig. 8(a) and (b)]. Fig. 8(c) shows the change in $|S_{21}|$ caused by wrapping the surface with the FSS. The curved FSS attenuates high-frequency EM waves by at least 10 dB from 5 to 10 GHz. The effect of the curved FSS on transmission is related to the transmission coefficient through the corresponding planar FSS under some conditions as shown below. These conditions decide the types of arbitrarily curved surfaces that the FSS can be wrapped on to provide EM shielding as demonstrated in the measurements. Consider a dipole placed outside a sphere formed by the FSS. The representation formula for the electric field inside the FSS is [16, Ch. 8]

$$\mathbf{E}(\mathbf{x}) = -\int_S dS'\,\hat{\mathbf{n}}' \cdot \big[\mathbf{H}(\mathbf{x}') \times \bar{\mathbf{G}}_e(\mathbf{x}', \mathbf{x}). + \mathbf{E}(\mathbf{x}') \times \bar{\mathbf{G}}_h(\mathbf{x}', \mathbf{x})\big] \quad (1)$$

where S is a surface just inside the FSS, $\mathbf{x}$ is any point inside S, $\hat{\mathbf{n}}'$ is the unit inward normal on the surface at the point $\mathbf{x}'$, and $\bar{\mathbf{G}}_e(\mathbf{x}', \mathbf{x})$ and $\bar{\mathbf{G}}_h(\mathbf{x}', \mathbf{x})$ are the electric and magnetic field dyadic Green's functions, respectively, for a unit dyadic current source radiating in unbounded medium. The far-field forms (we assume that r_2, defined below, is greater than the wavelength) for the dyadic Green's functions are as follows:

$$\bar{\mathbf{G}}_e(\mathbf{x}', \mathbf{x}) = -j\omega\mu \left(\bar{\mathbf{I}} - \hat{\mathbf{r}}_2\hat{\mathbf{r}}_2\right) \frac{e^{-jkr_2}}{4\pi r_2} \tag{2}$$

$$\bar{\mathbf{G}}_h(\mathbf{x}', \mathbf{x}) = -jk \left(\hat{\mathbf{r}}_2 \times \bar{\mathbf{I}}\right) \frac{e^{-jkr_2}}{4\pi r_2} \tag{3}$$

where ω is the radian frequency, k is the wave number, μ is the magnetic permeability, $\bar{\mathbf{I}}$ is the unit dyadic, $\hat{\mathbf{r}}_2$ is the unit vector in the direction of $\mathbf{x}' - \mathbf{x}$, and $r_2 = |\mathbf{x}' - \mathbf{x}|$. Assuming that the FSS is in the far field of the dipole, we can write the electric and magnetic fields just inside the FSS using the ray theory approximation as follows:

$$\mathbf{E}(\mathbf{x}') = jk\eta\, I_0 l\, T(\mathbf{x}') \sin\theta\, \frac{e^{-jkr_1}}{4\pi r_1}\hat{\boldsymbol{\gamma}} = E_\gamma \hat{\boldsymbol{\gamma}} \tag{4}$$

$$\mathbf{H}(\mathbf{x}') = \frac{E_\gamma}{\eta}\hat{\boldsymbol{\zeta}} \tag{5}$$

where the spherical coordinate system centered at the dipole is assumed, η is the free-space impedance, $I_0 l$ is the strength of the dipole, r_1 is the radial distance from the dipole, θ is the polar angle, $T(\mathbf{x}')$ is the plane wave transmission coefficient through an infinite planar FSS lying on the tangent plane at the point $\mathbf{x}'$ on the surface S, and $\hat{\boldsymbol{\gamma}}$ and $\hat{\boldsymbol{\zeta}}$ are unit vectors in the direction of polarization of the electric and magnetic fields, respectively. Although not explicitly indicated, the transmission coefficient $T(\mathbf{x}')$, and the unit vectors $\hat{\boldsymbol{\gamma}}$ and $\hat{\boldsymbol{\zeta}}$, are functions of the angle of incidence and the orientation of the principal directions of the FSS, in general. In writing the above equations, the assumption is that a plane wave incident on a planar FSS is transmitted as a plane wave, which holds true only when there are no grating lobes. If the wavelength is large compared to the element periodicity of the FSS, this condition on grating lobes is satisfied. Therefore, the assumption is that although the wavelength is smaller than r_2, it is not small enough that grating lobes come into play. Substituting the above expressions in the formula for the electric field inside the FSS, we have

$$\mathbf{E}(\mathbf{x}) = -\tfrac{k^2\eta I_0 l}{(4\pi)^2} \int_S dS'\, T(\mathbf{x}') \sin\theta \frac{e^{-jk(r_1+r_2)}}{r_1 r_2}\hat{\mathbf{n}}' \cdot \left[\hat{\boldsymbol{\gamma}} \times (\hat{\mathbf{r}}_2 \times \bar{\mathbf{I}}) + \hat{\boldsymbol{\zeta}} \times (\bar{\mathbf{I}} - \hat{\mathbf{r}}_2\hat{\mathbf{r}}_2)\right]. \tag{6}$$

Since the exponential $e^{-jk(r_1+r_2)}$ varies very fast compared to the other terms in the integrand, the above integral can be evaluated using the stationary phase approach. After evaluation of the integral using the stationary phase approach, the electric field becomes proportional to $T(\mathbf{x'}_0)$, where $\mathbf{x'}_0$ is the stationary phase point. The phase term in the integrand $k(r_1 + r_2)$ is minimum when the point $\mathbf{x}'$ lies on the straight line connecting $\mathbf{x}$ to the center of the dipole. The stationary phase point, therefore, lies at the intersection of the FSS with the line connecting $\mathbf{x}$ to the center of the dipole. If the point $\mathbf{x}$ is the center of the sphere formed by the FSS, then $T(\mathbf{x'}_0)$ is the transmission coefficient at normal incidence. Although the above equation is derived for a spherically curved FSS, it applies even to arbitrarily curved FSSs, whenever the curvature of the FSS allows the application of ray theory approximation as mentioned above. Then, the electric field inside the FSS is approximately proportional to the transmission coefficient through the corresponding planar FSS, albeit at some incident angle, which is decided by the stationary phase approximation. Assuming the antennas used in the measurements to be small, the angle of incidence at the stationary phase point is 0° for both the measurements. Therefore, the observed transmission response is approximately proportional to the transmission coefficient of the planar FSS at normal incidence. Finally, it should be noted that changing the positions of the antennas changes the angle of incidence at the stationary phase point, which can degrade the performance of the FSS. Although not done here, this can be compensated by designing the FSS for angular stability.

IV. Conclusion

A square-patch conformal FSS has been demonstrated by embedding EGaIn in an elastomer. The stretchability of the substrate allows the FSS to be wrapped on doubly curved surfaces. The FSS exhibits a low-pass transmission response when wrapped on cylindrical or spherical radomes and is, therefore, effective in reducing EM interference in the X-band.

Acknowledgment

The authors would like to thank Dr. H. Ceylan for helpful discussion in potential applications, M. Yang for his assistance in device fabrications, and Dr. R. J. Weber for his help with device measurements.

References

[1] B. Munk, *Frequency Selective Surfaces: Theory and Design.* New York, NY, USA: Wiley, 2000.

[2] M. Safari *et al.*, "X-band tunable frequency selective surface using MEMS capacitive loads," *IEEE Trans. Antennas Propag.*, vol. 63, no. 3, pp. 1014–1021, Mar. 2015.

[3] L. Dong *et al.*, "Design and fabrication of single-chip a-Si TFT-based uncooled infrared sensors," *Sens. Actuators A*, vol. 116, no. 2, pp. 257–263, 2004.

[4] F. C. Seman *et al.*, "Characterisation of copper nanoparticle ink printed FSS for cellular signals suppression," *Prog. Electromagn. Res. Lett.*, vol. 60, pp. 101–106, 2016.

[5] A. A. Dewani *et al.*, "Miniaturised meandered square frequency selective surface on a thin flexible dielectric with selective transmission," *Flexible Printed Electron.*, vol. 1, no. 2, 2016, Art. no. 025001.

[6] G. Coutts *et al.*, "A MEMS-tunable frequency-selective surface monolithically integrated on a flexible substrate," in *Proc. IEEE MTT-S Int. Microw. Symp.*, 2007, pp. 497–500.

[7] R. Seager *et al.*, "Fabric based frequency selective surfaces using weaving and screen printing," *Electron. Lett.*, vol. 49, no. 24, pp. 1507–1509, 2013.

[8] M. Nauman *et al.*, "A miniaturized flexible frequency selective surface for X-band applications," *IEEE Trans. Electromagn. Compat.*, vol. 58, no. 2, pp. 419–428, Apr. 2016.

[9] J.-H. Choi *et al.*, "An electroactive, tunable, and frequency selective surface utilizing highly stretchable dielectric elastomer actuators," *Small*, vol. 12, no. 14, pp. 1840–1846, 2016.

[10] S. Yang *et al.*, "From flexible and stretchable meta-atom to metamaterial: A wearable microwave meta-skin with tunable frequency selective and cloaking effects," *Sci. Rep.*, vol. 6, 2016, Art. no. 21921.

[11] P. Liu *et al.*, "Tunable meta-atom using liquid metal embedded in stretchable polymer," *J. Appl. Phys.*, vol. 118, no. 1, 2015, Art. no. 014504.

[12] P. Liu *et al.*, "Directivity-reconfigurable wideband two-arm spiral antenna," *IEEE Antennas Wireless Propag. Lett.*, vol. 16, pp. 66–69, 2017.

[13] G. Gerini and L. Zappelli, "Multilayer array antennas with integrated frequency selective surfaces conformal to a circular cylindrical surface," *IEEE Trans. Antennas Propag*, vol. 53, no. 6, pp. 2020–2030, Jun. 2005.

[14] L. B. Whitbourn and R. C. Compton, "Equivalent-circuit formulas for metal grid reflectors at a dielectric boundary," *Appl. Opt.*, vol. 24, no. 2, pp. 217–220, 1985.

[15] "Ecoflex series—smooth-on," Jun. 25, 2017. [Online]. Available: https://www.smooth-on.com/tb/files/ECOFLEX_SERIES_TB.pdf

[16] W. C. Chew, *Waves and Fields in Inhomogeneous Media*, vol. 522. Piscataway, NJ, USA: IEEE Press, 1995.